Original Article

PMP

Progress in Medical Physics 32(4), December 2021
https://doi.org/10.14316/pmp.2021.32.4.165
eISSN 2508-4453

Effect of Total Collimation Width on Relative Electron Density, Effective Atomic Number, and Stopping Power Ratio Acquired by Dual-Layer Dual-Energy Computed Tomography

Seongmoon Jung[1,2,3], Bitbyeol Kim[1], Euntaek Yoon[4], Jung-in Kim[1,2,3], Jong Min Park[1,2,3,4,5,6], Chang Heon Choi[1,2,3]

[1]Department of Radiation Oncology, Seoul National University Hospital, [2]Institute of Radiation Medicine, Seoul National University Medical Research Center, [3]Biomedical Research Institute, Seoul National University Hospital, [4]Interdisciplinary Program in Bioengineering, Seoul National University, [5]Department of Radiation Oncology, Seoul National University College of Medicine, Seoul, [6]Robotics Research Laboratory for Extreme Environments, Advanced Institute of Convergence Technology, Suwon, Korea

Received 5 December 2021
Revised 10 December 2021
Accepted 14 December 2021

Corresponding author
Chang Heon Choi
(dm140@snu.ac.kr)
Tel: 82-2-2072-3573
Fax: 82-2-765-3317

Purpose: This study aimed to evaluate the effect of collimator width on effective atomic number (EAN), relative electron density (RED), and stopping power ratio (SPR) measured by dual-layer dual-energy computed tomography (DL-DECT).

Methods: CIRS electron density calibration phantoms with two different arrangements of material plugs were scanned by DL-DECT with two different collimator widths. The first phantom included two dense bone plugs, while the second excluded dense bone plugs. The collimator widths selected were 64 mm×0.625 mm for wider collimators and 16 mm×0.625 mm for narrow collimators. The scanning parameters were 120 kVp, 0.33 second gantry rotation, 3 mm slice thickness, B reconstruction filter, and spectral level 4. An image analysis portal system provided by a computed tomography (CT) manufacturer was used to derive the EAN and RED of the phantoms from the combination of low energy and high energy CT images. The EAN and RED were compared between the images scanned using the two different collimation widths.

Results: The CT images with the wider collimation width generated more severe artifacts, particularly with high-density material (i.e., dense bone). RED and EAN for tissues (excluding lung and bones) with the wider collimation width showed significant relative differences compared to the theoretical value (4.5% for RED and 20.6% for EAN), while those with the narrow collimation width were closer to the theoretical value of each material (2.2% for EAN and 2.3% for RED). Scanning with narrow collimation width increased the accuracy of SPR estimation even with high-density bone plugs in the phantom.

Conclusions: The effect of CT collimation width on EAN, RED, and SPR measured by DL-DECT was evaluated. In order to improve the accuracy of the measured EAN, RED, and SPR by DL-DECT, CT scanning should be performed using narrow collimation widths.

Keywords: Dual-layer dual-energy computed tomography, Collimation width, Cone-beam artifact, Effective atomic number, Relative electron density, Stopping power ratio

Introduction

Over the last few decades, the technical improvement of dual-energy computed tomography (DECT) has led many researchers to suggest the utility and implementation of DECT to improve the accuracy of dose calculation in treatment planning systems as well as the use of Monte Carlo simulation for proton and heavy ion therapy [1,2]. By pairing a low energy and a high energy CT image, DECT can estimate more accurate relative electron density (RED), effective atomic number (EAN), and stopping power ratio (SPR) than conventional single energy CT (SECT) [1,3]. More recently, several studies using dual-layer DECT (DL-DECT) have shown it to accurately estimate RED and EAN [3,4,5]. Particularly, Ohira et al. [4] have examined the effects on estimation accuracy of different scanning parameters such as gantry rotation time, volume CT dose index ($CTDI_{vol}$), and tube current.

In clinical practice with most multi-detector CTs, a wide collimation width is preferred due to the faster scan time [6]. However, cone-beam artifacts are often observed with wide collimation widths and multiple rows of detectors [6,7]. This artifact can be severe with high-density materials such as dense bone and metal implants and this has crucial effects on dose calculation in radiation therapy planning.

This study aims to evaluate the effect of cone-beam artifacts on the accuracy of RED, EAN, and SPR. Since cone-beam artifacts are caused by wide collimation widths and high-density materials, we scanned an electron density phantom (Model 062M; CIRS Inc., Norfolk, VA, USA) using both wide and narrow collimation widths. The RED, EAN, and SPR were compared between the two images. We also investigated the effects of high-density material on cone-beam artifacts by comparing the CT images, RED, EAN, and SPR of phantoms with and without dense bone plugs.

Materials and Methods

1. CT scanning of phantoms

A CIRS phantom with two different arrangements including eight different materials and a total of sixteen plugs was scanned with DL-DECT (IQon Spectral CT; Philips, Best, Netherlands). The material information including composition, physical density, RED, and EAN is shown in Table 1 [8,9]. As shown in Fig. 1, one of the two arrangements (Arr1) included dense bone plugs, while the other (Arr2) did not. For Arr2, two empty holes were left in place of the dense bone plugs and we did not evaluate those regions.

The collimator widths selected were 64 mm×0.625 mm for wider collimation and 16 mm×0.625 mm for narrow collimation. The other scanning parameters were 120 kVp for the tube voltage, 0.33 second gantry rotation, 3 mm slice thickness, B reconstruction filter, and spectral level 4. The pitch factor, tube current, exposure, and $CTDI_{vol}$ for the scanning of the phantoms with the different collimation widths are shown in Table 2.

2. Acquisition of EAN, RED, and SPR

The image analysis portal system, IntelliSpace Portal (Philips), provided by the CT manufacturer, was used to

Table 1. Material information of CIRS phantom

Material	Material composition (%)								Theoretical value		
	H	C	N	O	P	Cl	Ca	Ba	Physical density	Relative electron density	Effective atomic number
Lung inhale	8.8	67.5	3.5	18.6	0	1.6	0	0	0.205	0.200	6.685
Lung exhale	8.9	66	2.4	20.4	0	0.6	1.7	0	0.507	0.496	7.231
Adipose	10	71.3	1.8	16.4	0	0.2	0.3	0	0.96	0.949	6.301
Breast	9.6	70.4	1.9	17	0	0.2	0.9	0	0.99	0.976	6.651
Muscle	9.1	69.7	2.1	16.8	0	0.1	2.2	0	1.06	1.04	7.249
Liver	9	69.5	2.1	17.1	0	0.1	2.2	0	1.07	1.052	7.258
Trabecular bone	7	56.3	2	22.7	3.3	0.2	8.5	0	1.16	1.117	9.833
Dense bone	5.7	40.8	1	25.9	8.3	0.1	17.9	0.3	1.53	1.456	12.963

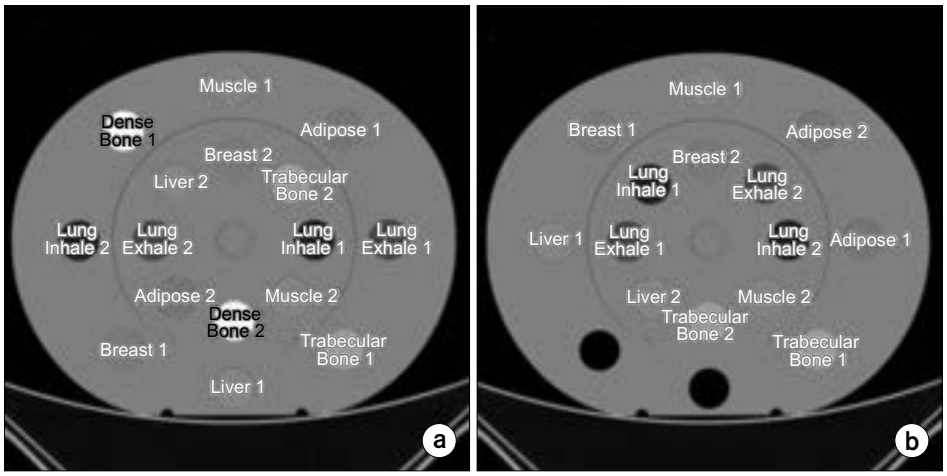

Fig. 1. Two arrangements of CIRS phantoms. (a) Arrangement 1 (Arr1) included two dense bone plugs. (b) Arrangement 2 (Arr2) had no dense bone plugs.

Table 2. Total collimator width, pitch factor, X-ray tube current, exposure time, and $CTDI_{vol}$ of computed tography scans for the central imaging plane of the phantom

Phantom with collimation width	Total collimator width (mm)	Pitch factor	Tube current (mA)	Exposure (mAs)	$CTDI_{vol}$ (mGy)
Arr1 with wide collimation	40	0.797	385	159	14.4
Arr1 with narrow collimation	10	0.812	380	154	19.0
Arr2 with wide collimation	40	0.797	353	146	13.2
Arr2 with narrow collimation	10	0.812	381	155	19.2

Arr, arrangement.

derive the EAN and RED of the phantoms from the combination of low energy (i.e., photoelectric image) and high energy (i.e., Compton image) CT images. The EAN and RED for each phantom and collimation width were analyzed for the defined region of interests (ROIs), which were 2.4 cm in diameter and 9 mm high (for three consecutive image slices). The SPR for each ROI was calculated with equation (1) using the measured EAN and RED. The derived SPR values for each material were then compared with the theoretical SPRs which were calculated using the same equation.

$$\mathrm{SPR} = \mathrm{RED} \times \frac{\ln\left[\frac{2m_e c^2}{I_m(1-\beta^2)}\right] - \beta^2}{\ln\left[\frac{2m_e c^2}{I_{water}(1-\beta^2)}\right] - \beta^2} \quad (1)$$

The EAN, RED, and SPR for each phantom and collimation width were then compared between the images with the wider and narrower collimation widths. The SPR were described by the difference between each theoretical and calculated SPR using the measured EAN and RED.

Results

CT images acquired by DL-DECT are shown in Fig. 2. Cone-beam artifacts were apparent in images with wide collimation width. Severe artifacts were particularly apparent near the high-density material (i.e., dense bone plugs). With narrow collimation CT imaging, the cone-beam artifacts were dramatically reduced.

Table 3 and 4 present the RED and EAN measured by DL-DECT with wide and narrow collimation for Arr1 and Arr2 and show the relative differences between the theoretical values and the measured values. For both wide and narrow collimation widths, the relative differences of RED and EAN for lung inhale and lung exhale were –8.5% to 8.1% for Arr1 and –6.7% to 8.7% for Arr2, respectively. For tissues such as adipose, breast, muscle, and liver, in Arr1, DL-DECT with narrow collimation showed values similar to the theoretical values (2.2% relative difference for EAN and 2.3% relative difference for RED). However, for DL-DECT with wide collimation, the relative differences with the aforementioned tissues increased up to 4.5% for RED and 20.6% for EAN. For

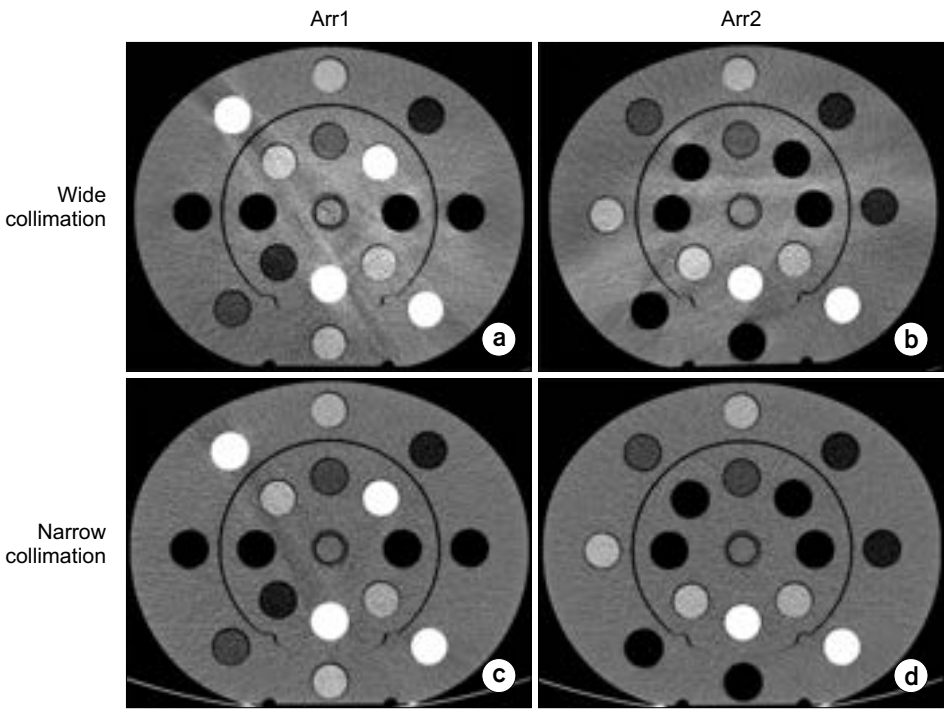

Fig. 2. Computed tomography (CT) images acquired with wide collimation for (a) phantom arrangement 1 (Arr1) and (b) arrangement 2 (Arr2). CT images acquired with narrow collimation for (c) phantom Arr1 and (d) phantom Arr2. Window width and level were 200 HU and 15 HU, respectively.

Table 3. RED and EAN for DL-DECT images with wide and narrow collimation for Arr1

Material	RED					EAN				
	Theoretical value	Wide collimation		Narrow collimation		Theoretical value	Wide collimation		Narrow collimation	
		Mean	R.D (%)	Mean	R.D (%)		Mean	R.D (%)	Mean	R.D (%)
Lung inhale 1	0.200	0.196	−2.1	0.205	2.5	6.685	5.417	−19.0	6.863	2.7
Lung inhale 2		0.209	4.5	0.205	2.5		5.000	−25.1	6.117	−8.5
Lung exhale 1	0.496	0.536	8.1	0.537	8.3	7.231	6.156	−14.9	7.322	1.3
Lung exhale 2		0.519	4.7	0.537	8.3		8.200	13.4	7.375	2.0
Adipose 1	0.949	0.977	2.9	0.955	0.6	6.301	5.092	−19.2	6.325	0.4
Adipose 2		0.967	1.9	0.955	0.6		6.051	−4.0	6.253	−0.8
Breast 1	0.976	0.999	2.3	0.983	0.7	6.651	6.146	−7.6	6.720	1.0
Breast 2		0.962	−1.4	0.982	0.6		8.022	20.6	6.788	2.1
Muscle 1	1.040	1.033	−0.7	1.042	0.2	7.249	7.905	9.1	7.411	2.2
Muscle 2		1.086	4.5	1.043	0.3		5.981	−17.5	7.309	0.8
Liver 1	1.052	1.028	−2.3	1.051	−0.1	7.258	8.120	11.9	7.373	1.6
Liver 2		1.054	0.1	1.049	−2.3		7.620	5.0	7.377	1.6
Trabecular bone 1	1.117	1.103	−1.2	1.094	−2.1	9.833	9.849	0.2	9.757	−0.8
Trabecular bone 2		1.086	−2.8	1.091	−2.3		10.540	7.2	9.851	0.2
Dense bone 1	1.456	1.396	−4.1	1.422	−2.3	12.963	13.418	3.5	12.773	−1.5
Dense bone 2		1.447	−0.7	1.427	−2.0		13.180	1.7	12.703	−2.0

RED, relative electron density; EAN, effective atomic number; DL-DECT, dual-layer dual-energy computed tomography; Arr, arrangement. R.D indicates the relative difference between theoretical values and the measured values.

dense material (i.e., dense bone), the accuracy of wide and narrow collimation was similar (−4.1% to 3.5%). For the tissues in Arr2 without dense bone plugs, the accuracy of EAN with wider collimation was greater than that in Arr1. However, narrow collimation still provided superior accuracy in the estimation of RED and EAN compared to wide collimation. With narrow collimation width, the relative difference of RED in Arr2 was within 0.8%, and the relative difference

Table 4. RED and EAN for DL-DECT images with wide collimation and narrow collimation for Arr2

Material	RED					EAN				
	Theoretical value	Wide collimation		Narrow collimation		Theoretical value	Wide collimation		Narrow collimation	
		Mean	R.D (%)	Mean	R.D (%)		Mean	R.D (%)	Mean	R.D (%)
Lung inhale 1	0.200	0.201	0.5	0.197	−1.5	6.685	5.049	−24.5	6.688	0.0
Lung inhale 2		0.200	0.2	0.209	4.5		5.590	−16.4	6.239	−6.7
Lung exhale 1	0.496	0.531	7.1	0.539	8.7	7.231	7.428	2.7	7.248	0.2
Lung exhale 2		0.530	6.9	0.536	8.1		7.635	5.6	7.347	1.6
Adipose 1	0.949	0.960	1.2	0.956	0.7	6.301	6.220	−1.3	6.263	−0.6
Adipose 2		0.955	0.6	0.954	0.5		6.374	1.2	6.376	1.2
Breast 1	0.976	0.984	0.8	0.984	0.8	6.651	6.735	1.3	6.721	1.1
Breast 2		0.983	0.7	0.982	0.6		7.093	6.7	6.763	1.7
Muscle 1	1.040	1.043	0.3	1.043	0.3	7.249	7.441	2.7	7.391	2.0
Muscle 2		1.044	0.4	1.043	0.3		7.594	4.7	7.329	1.1
Liver 1	1.052	1.053	0.1	1.050	−0.2	7.258	7.343	1.2	7.397	1.9
Liver 2		1.044	−0.8	1.049	0.3		8.174	12.6	7.369	1.5
Trabecular bone 1	1.117	1.093	−2.2	1.094	−2.1	9.833	10.044	2.1	9.774	−0.6
Trabecular bone 2		1.078	−3.5	1.095	−2.0		10.440	6.2	9.754	−0.8

RED, relative electron density; EAN, effective atomic number; DL-DECT, dual-layer dual-energy computed tomography; Arr, arrangement. R.D indicates the relative difference between theoretical values and the measured values.

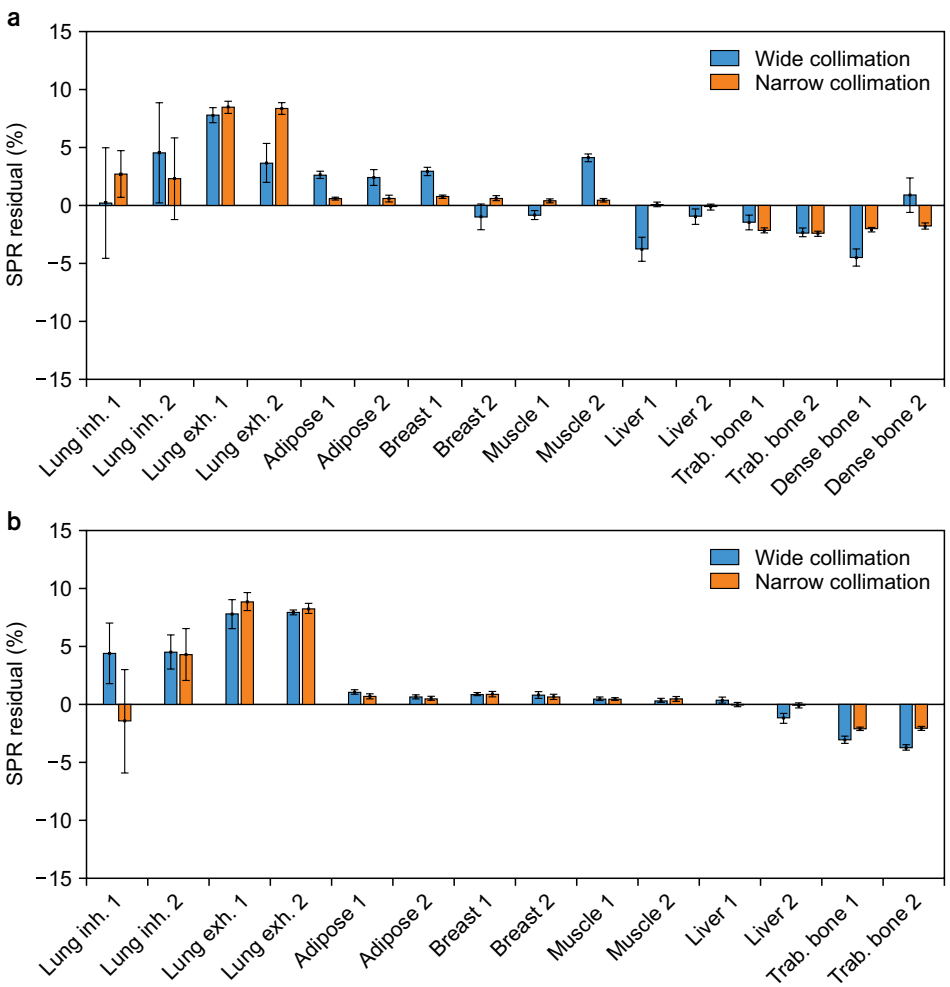

Fig. 3. Stopping power ratio (SPR) residual for (a) arrangement 1 (Arr1) and (b) arrangement 2 (Arr2) for comparison of the accuracy of SPR estimation. inh., inhale; exh., exhale; trab. trabecular.

of EAN was within 2.0%.

The SPR residuals for Arr1 and Arr2 are shown in Fig. 3. Due to the limited accuracy of RED and EAN, the SPR residuals for lung inhale and lung exhale from both wide and narrow collimations were up to 9%. In addition, due to the severe cone-beam artifacts in Arr2, the SPR residual had large variations between the materials. Narrow collimation increased the accuracy of SPR estimation even with high-density bone plugs in the phantom. With no high-density material in the object, scanning with wide and narrow collimations showed similar results.

Discussion

We evaluated the negative impact of cone-beam artifacts on the estimation of RED, EAN, and SPR measured by DL-DECT by varying the collimation width of CT scans. Severe artifacts in the images acquired with wide collimation widths were observed and these affected the HUs in both low energy (photoelectric) and high energy (Compton) CT images. Since the RED and EAN were derived by the relation between the low energy CT images and high energy CT images [3,4,5], variation in HUs reduced the accuracy of estimation of RED, EAN, and SPR. Inaccurate SPR can result in a critical range uncertainty error [10,11]. The proton range uncertainty from the conventional HU conversion method (i.e., stoichiometric conversion) has been reported to be up to 1.8% for bone and 1.1% for soft tissues, corresponding to 1.3 mm. [12]. Wohlfahrt et al. [11] have demonstrated that CT-related uncertainties can be reduced using DECT instead of SECT, resulting in decreased dependence of SPR prediction on beam hardening. For the fast scanning of patients in clinical practice, wide collimation widths are commonly used. However, for radiation therapy treatment planning purposes, cone-beam artifacts can cause severe dose calculation errors in proton and heavy ion radiotherapy. Cone-beam artifacts can be reduced using narrow collimation widths or slower pitch factors. Furthermore, since cone-beam artifacts are more prominent in the periphery of the field of view (FOV), it is important to align the center of the imaging volume with the center of the FOV [6].

Conclusions

Cone-beam artifacts resulting from wide CT collimation widths in DL-DECT may significantly affect the accuracy of EAN, RED, and SPR estimations. For improved accuracy, CT scanning should be performed with narrow collimation widths or increased pitch factor.

Acknowledgements

This study was supported by a grant by a National Research Foundation of Korea (NRF) grant funded by the Korean government (MSIP) (No.2019M2A2B4095117, No.2019M2A2B4095126, No.2019M2A2B4096540, and No.2020R1F1A1073430).

Conflicts of Interest

The authors have nothing to disclose.

Availability of Data and Materials

All relevant data are within the paper and its Supporting Information files.

Author Contributions

Conceptualization: Seongmoon Jung. Data curation: Euntaek Yoon. Formal analysis: Bitbyeol Kim and Euntaek Yoon. Funding acquisition: Seongmoon Jung, Jong Min Park, and Chang Heon Choi. Investigation: Bitbyeol Kim and Euntaek Yoon. Methodology: Seongmoon Jung and Jung-in Kim. Project administration: Jong Min Park. Resources: Chang Heon Choi. Software: Seongmoon Jung and Bitbyeol Kim. Supervision: Chang Heon Choi. Validation: Jung-in Kim. Visualization: Bitbyeol Kim. Writing–original draft: Seongmoon Jung. Writing–review & editing: Chang Heon Choi.

References

1. Faller FK, Mein S, Ackermann B, Debus J, Stiller W, Mairani A. Pre-clinical evaluation of dual-layer spectral computed

tomography-based stopping power prediction for particle therapy planning at the Heidelberg Ion Beam Therapy Center. Phys Med Biol. 2020;65:095007.
2. Jung S, Kim B, Kim JI, Park JM, Choi CH. Deriving the effective atomic number with a dual-energy image set acquired by the Big Bore CT simulator. J Radiat Prot Res. 2020;45:171-177.
3. Hua CH, Shapira N, Merchant TE, Klahr P, Yagil Y. Accuracy of electron density, effective atomic number, and iodine concentration determination with a dual-layer dual-energy computed tomography system. Med Phys. 2018;45:2486-2497.
4. Ohira S, Washio H, Yagi M, Karino T, Nakamura K, Ueda Y, et al. Estimation of electron density, effective atomic number and stopping power ratio using dual-layer computed tomography for radiotherapy treatment planning. Phys Med. 2018;56:34-40.
5. Mei K, Ehn S, Oechsner M, Kopp FK, Pfeiffer D, Fingerle AA, et al. Dual-layer spectral computed tomography: measuring relative electron density. Eur Radiol Exp. 2018;2:20.
6. Yu L, McCollough CH, Leng S, Kofler JM. 2011 Joint AAPM/COMP meeting program. Optimization of image acquisition and reconstruction in multi-slice CT. Med Phys. 2011;38(6Pt33):3822.
7. Edward Boas F, Fleischmann D. CT artifacts: causes and reduction techniques. Imaging Med. 2012;4:229-240.
8. Almeida IP, Schyns LEJR, Vaniqui A, van der Heyden B, Dedes G, Resch AF, et al. Monte Carlo proton dose calculations using a radiotherapy specific dual-energy CT scanner for tissue segmentation and range assessment. Phys Med Biol. 2018;63:115008.
9. Landry G, Parodi K, Wildberger JE, Verhaegen F. Deriving concentrations of oxygen and carbon in human tissues using single- and dual-energy CT for ion therapy applications. Phys Med Biol. 2013;58:5029-5048.
10. Paganetti H. Range uncertainties in proton therapy and the role of Monte Carlo simulations. Phys Med Biol. 2012;57:R99-R117.
11. Wohlfahrt P, Möhler C, Hietschold V, Menkel S, Greilich S, Krause M, et al. Clinical implementation of dual-energy CT for proton treatment planning on pseudomonoenergetic CT scans. Int J Radiat Oncol Biol Phys. 2017;97:427-434.
12. Schaffner B, Pedroni E. The precision of proton range calculations in proton radiotherapy treatment planning: experimental verification of the relation between CT-HU and proton stopping power. Phys Med Biol. 1998;43:1579-1592.